Proceedings of the IX International Conference ION 2012, Kazimierz Dolny, Poland, June 25–28, 2012

Ion Beam Synthesis of InAs Nanocrystals in Si: Influence of Thin Surface Oxide Layers

F. Komarov[a,*], L. Vlasukova[a], O. Milchanin[a], M. Greben[a], A. Komarov[a], A. Mudryi[b], W. Wesch[c], E. Wendler[c], J. Zuk[d], M. Kulik[d] and G. Ismailova[e]

[a]Belarusian State University, Nezavisimosti ave. 4, 220030 Minsk, Belarus

[b]Scientific and Practical Materials Research Center, National Academy of Sciences of Belarus P. Brovki Str. 17, 220072 Minsk, Belarus

[c]Institut für Festkörperphysik, Friedrich-Schiller-Universität Jena, Max-Wien-Platz 1, D-07743 Jena, Germany

[d]Maria Curie-Skłodowska University, pl. M. Curie-Skłodowskiej 1, 20-031 Lublin, Poland

[e]Al-Farabi Kazakh National University, 71 al-Farabi ave., 050040 Almaty, Kazakhstan

Nanosized crystallites have been synthesized in the Si and SiO_2/Si structures by means of As (170 keV, 3.2×10^{16} cm^{-2}) and In (250 keV, 2.8×10^{16} cm^{-2}) implantation at 25 °C and 500 °C and subsequent annealing at 1050 °C for 3 min. The Rutherford backscattering, transmission electron microscopy, and photoluminescence techniques were used to analyse the impurity distribution as well as the structural and optical characteristics of the implanted layers. It was found that oxidation of samples before thermal treatment significantly reduced the As and In losses. A broad band in the region of 1.2–1.5 μm was detected in the photoluminescence spectra. The highest photoluminescence yield for the samples after "hot" implantation and annealing was obtained. Anodic oxidation of the implanted samples before annealing results in the additional increase of photoluminescence yield.

DOI: 10.12693/APhysPolA.123.809

PACS: 61.80.−x, 61.72.Ff, 63.20.−e, 78.66.−w

1. Introduction

One of the most challenging problems of material research is creating optoelectronic devices based on silicon technology. Silicon is an inefficient emitter of light. It is possible to improve optical properties of silicon by forming of a low-dimensional system in the silicon bulk. The synthesis of A^3B^5 quantum dots (QDs) in crystalline Si is a promising approach of significant interest for application in light emitting diodes and photodetectors operating in the infrared (IR) range.

InAs clusters were formed on the (100) by the molecular beam epitaxy (MBE)-technique [1, 2]. The sample with these clusters shows photoluminescence in the 1.3 μm region, which was tentatively attributed to the recombination of excitons localised in the ordered regions. In this paper we report the alternative technique for fabricating of III–V quantum dots: ion-beam synthesis of nanocrystals by means of ion implantation followed by thermal treatment. Modifying the regime of annealing or changing the order in which the different ion species are implanted may provide a way to control the size and crystalline quality of the compound precipitates formed. The formation of InAs nanoclusters using this method in SiO_2 and Si [3–5] was reported. Unfortunately, thermal processing of implanted crystals results not only in precipitation and radiation damage recovery, but also in a net loss of implanted ions because of diffusion that is favoured at elevated temperature.

The purpose of this paper is to investigate the influence of thin surface SiO_2 layer grown on the Si wafer on embedded impurities (As and In) losses during the post-implantation thermal processing and to analyse the structural and optical properties of the implanted samples.

2. Experimental

We used two sets of samples in this paper. The samples from the first set were cut from the thermally oxidized n-type Si (100) wafer. The thickness of thermal SiO_2 was equal to 40 nm. The samples from the second set were cut from the p-type Si (111) wafer. After that two sets of samples were implanted with As^+ (170 keV, 3.2×10^{16} cm^{-2}) and then In^+ (250 keV, 2.8×10^{16} cm^{-2}) ions at 25 and 500 °C. After implantation a part of Si (111) samples was electrochemically oxidized (thickness of the oxide layer was 100 ± 30 nm) in order to prevent impurity loss during subsequent annealing. Finally, rapid thermal annealing at 1050 °C for 3 min in an inert ambient was carried out in order to restore crystalline structure of the implanted samples.

The Rutherford backscattering spectrometry in combination with the channelling technique (RBS/C) with 1.5 MeV and 2.5 MeV He^+ was used to analyse depth distribution of the implanted atoms as well as to evaluate damage of the implanted material. The depth profiles of the implanted ions were obtained by computer simulation of spectra until they coincided completely with the

*corresponding author; e-mail: komarovf@bsu.by

experimental spectra which were recorded at two angles of incidence of the helium ions into the samples (0° and 50°). The structure of the implanted samples was studied by means of transmission electron microscopy (TEM) in the plan-view (PV) geometry. The TEM investigations were performed using a Hitachi H-800 instrument operating at 200 keV. The optical properties of samples were investigated by low temperature photoluminescence (PL). PL spectra were taken in the spectral region of 1700 to 1000 nm wavelength. During the measurements the samples were mounted in a liquid He immersion cryostat. The 514.5 nm line of an argon ion laser was used to induce PL. The luminescence was dispersed by a 0.6 m grating monochromator and detected by a cooled InGaAs detector.

3. Results and discussion

Figure 1a presents the depth profiles of As and In atoms in the as-implanted samples with 40 nm oxide layer before implantation simulated using the SRIM'12 and Beam2HD [6] computer codes. The SRIM code allows user only to estimate the coefficient of sputtering of the target atoms, but it does not take into account ion beam sputtering of the target during implantation in the final depth distribution of the considered impurity. To overcome this problem we use the Beam2HD code to simulate depth distribution of As and In atoms considering sputtering and to estimate the thickness of the sputtered layer. About 10 nm of SiO_2 material was sputtered during ion implantation in accordance with this simulation code. Therefore the data obtained from SRIM were shifted on 10 nm towards the surface (Fig. 1a). The comparison of SRIM and Beam2HD simulations indicates a small difference between them in the concentration maxima of impurities only. Both of these programs do not take into account the temperature of implantation and these simulated results are close to the experimental depth profiles of implanted species for low temperature implantation only (for example, $T_{\mathrm{imp}} = 25\,^{\circ}\mathrm{C}$ [7]).

The calculation of As and In depth concentration profiles in Si by the RBS method with low He^+ energies (< 2 MeV) is complicated because of the overlapping peaks from the implanted impurities. We estimated the necessary energy of He beam to completely resolve the yield of backscattered helium ions from As and In in the RBS spectra. Thus, we measured the RBS spectra with 2.5 MeV He^+ ions at two angles of the incidence beam onto the sample (0° and 50°) to improve accuracy of fitting spectra (Fig. 1c). The depth profiles were calculated by manual simulation of the spectra using the HEAD DOS code and automatically fitting of the spectra using the new generation code WinDF [8] until the simulated spectra coincided completely with the experimental spectra (Fig. 1b–d). Figure 1d presents the comparison of As and In depth distributions obtained from these programs. The calculation results by two programs (WinDF and HEAD) show close resemblance. One can see that

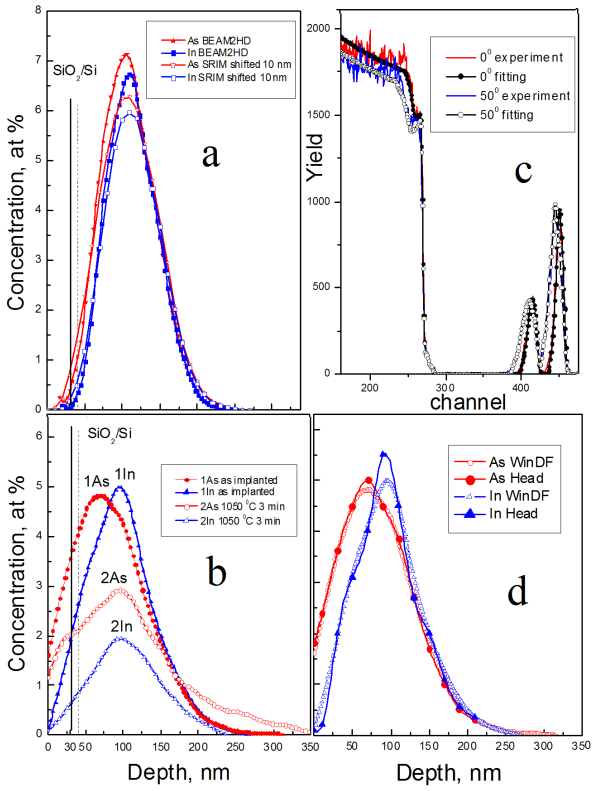

Fig. 1. Simulated (SRIM 2012 and Beam2HD) (a) and calculated from the RBS spectra (b,d) depth profiles of impurities in SiO_2/Si structure, implanted with As (170 keV, 3.2×10^{16} cm^{-2}) and In (250 keV, 2.8×10^{16} cm^{-2}) ions at 500 °C. As-implanted sample: experimental and fitted using WinDF code RBS spectra (c) and calculated In and As depth profiles (b-1, d); an annealed sample (b-2).

the "hot" conditions of implantation lead to depth profiles broadening and to reduction of impurity concentration in comparison with the simulated data (Fig. 1a,b). This effect is weaker for In than for As. The calculated loss of As and In atoms during "hot" implantation is equal to 7% and 5%, respectively. The high-fluence co-implantation of heavy ions such as As and In into the silicon matrix leads to creation of the system containing high concentrations of implanted species as well as high densities of radiation defect complexes. The calculations [9] have not predicted any noticeable impurity thermal diffusion due to equilibrium thermal diffusion at the implantation temperature of 500 °C. The impurity redistribution under the influence of equilibrium thermal diffusion starts at $T_{\mathrm{imp}} = 900\,^{\circ}\mathrm{C}$ only. Therefore, the embedded species redistribution experimentally observed under "hot" implantation conditions resulted from non-equilibrium radiation-enhanced diffusion caused by the migration of "impurity atom–radiation defect". Postimplantation annealing comes to decomposition of complex structure defects (as microtwins and dislocation loops) resulting in generation of a great number of point defects

such as interstitial silicon atoms. It might stimulate the diffusion redistribution of implanted impurity by means of the diffusion of complexes "interstitial silicon atom + embedded impurity" via interstitial mechanism.

One can see from Fig. 1a,b that the depth maxima of As and In concentrations substantially moved toward the surface and are located at different depths after the implantation procedure (As concentration maximum is near 70 nm, in the case of In — near 95 nm). This effect of impurity redistribution towards the surface as the most effective sink of defects during "hot" implantation was observed in our previous work for the samples without the oxide film, but the displacement of the depth profiles was considerably smaller [7]. Thus, we can assume that the presence of thin oxide layer on the top of the sample enhances redistribution of impurities during "hot" implantation. In spite of the depth separation of As and In concentration maxima in the as-implanted samples, subsequent thermal annealing results in convergence of the maxima of impurity concentration to the same depth. We can suppose that this converging of impurity depth maxima during thermal treatment is caused by InAs nanoclusters formation in the silicon matrix. The impurity which is bounded in nanoclusters becomes inactive to diffuse. The most effective cluster formation takes place in the area of overlapping depth profiles of different impurities. The calculated losses of As and In atoms after implantation at $T_{\text{imp}} = 500\,^{\circ}\text{C}$ and annealing are equal to 30% and 60%, respectively (Fig. 1b). One can see As piles up at the interface SiO_2/Si layer (Fig. 1b) [10].

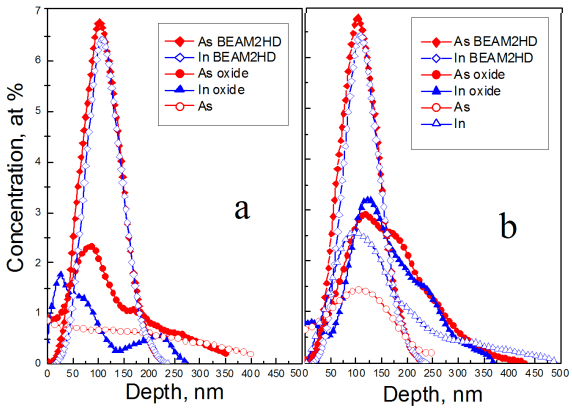

Fig. 2. Simulated (Beam2HD) and calculated from RBS spectra depth profiles of As and In atoms in Si (111) implanted at 25 (a) and 500 °C (b) and annealed. A part of samples was anodized before annealing.

Figure 2a,b presents the concentration profiles of As and In implanted in p-doped Si (111). One can see that oxidation of the samples before annealing reduces impurity losses. Indeed, the calculations show that in the case of $T_{\text{imp}} = 25\,^{\circ}\text{C}$ and subsequent annealing the oxide film presence reduces the loss of As to 25% and In to 35% (Fig. 2a). In the case of implantation at 500 °C and annealing the oxide surface layer reduces the loss of As to 50% and In to 10% (Fig. 2b). Moreover, one can see from Fig. 2a,b, that the oxide film decreases the broadening of depth profiles of the implanted species. In the case of implantation at room temperature oxidation leads to bimodal distribution of In: the first peak was formed in the SiO_2 layer because of non-equilibrium diffusion during "hot" implantation and post-implantation annealing, another one is located in Si near In ions projected range R_{p} (Fig. 2a). In atoms were not detected for sample without the oxide film at the surface under this treatment.

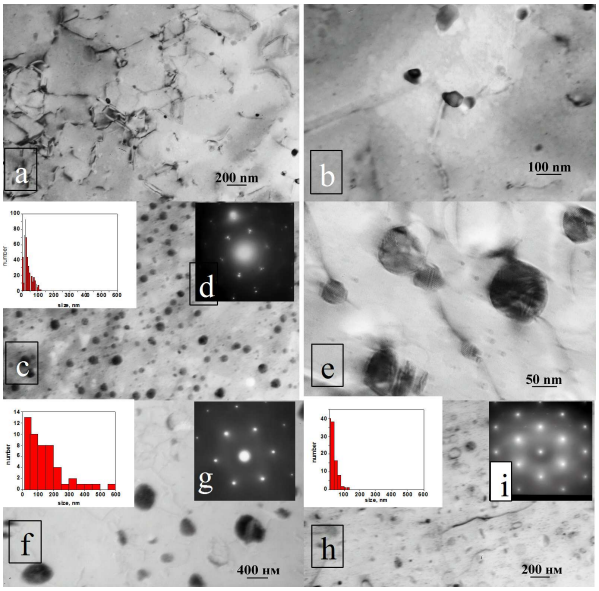

Fig. 3. Bright-field TEM-images (a,b,c,e,f,h) and microdiffraction patterns (d,g,i) from Si (a,b,c,e) and SiO_2/Si (f,h) after implantation at 25 °C (a,b,f) and 500 °C (c,e,h), anodic oxidation (f,h) and annealing.

Figure 3 shows the TEM-images of the precipitates for the annealed samples. One can see the faceted nanocrystals of the sizes from 2 to 600 nm. The crystalline nature of the precipitates is proved by the presence of the Moiré fringe patterns in the TEM images (Fig. 3e). In our previous work [5] we have analyzed the distance between the Moiré fringes and obtained good agreement for the superposition of InAs and Si {220} planes. Thus, a layer with the InAs crystallites is formed in the annealed samples. It should be noted that "hot" implantation at the elevated temperature results in narrower size distribution of nanocrystals from about 2 to 115–140 nm (depending on the presence of surface oxide film) (insets in Fig. 3c,f,h). The implantation at $T_{\text{imp}} = 25\,^{\circ}\text{C}$ (inset in Fig. 3f) leads to a broader nanocrystal size distribution and larger average nanocrystal sizes in comparison with $T_{\text{imp}} = 500\,^{\circ}\text{C}$ (inset in Fig. 3c,h). It is possible to estimate crystalline structure quality and to evaluate the percentage of impurity embedded into the silicon lattice sites by comparing random and aligned RBS spectra of

the implanted samples. Our calculations show that only 16% of the implanted impurity atoms are incorporated into the silicon lattice sites in the case of the sample after "hot" implantation and annealing. Oxidation of this sample before thermal treatment results in 65% of As and In atoms incorporated into the regular lattice sites of silicon. This indicates that the presence of an oxide film on the sample top before thermal treatment leads to more intensive impurity embedding into the silicon regular lattice sites. Impurity atoms incorporated into the silicon lattice sites do not participate in the cluster formation and that is why the average nanocluster size is smaller in the case of the sample with the oxide layer (inset in Fig. 3c,h).

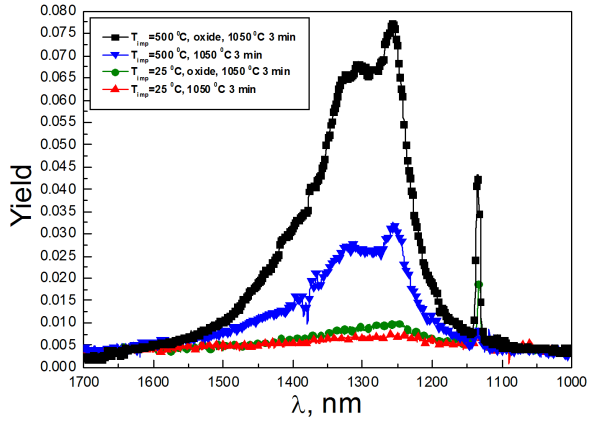

Fig. 4. PL spectra of SiO_2/Si and Si samples after implantation at 25 and 500 °C and annealing.

The surface region of the "hot" implanted, oxidized and annealed sample contains a lot of dislocation loops, microtwins and little size precipitates (Fig. 3h,i). However, photoluminescence yield from this sample is maximal in comparison with the other samples. All the PL spectra of the implanted samples can be characterized with a narrow line of exciton emission in Si at 1135 nm and a broad band at 1.15–1.6 μm (Fig. 4). A similar band was observed earlier in the PL spectra of InAs nanocrystals grown on the Si wafers by MBE [1] or synthesized by high-fluence ion implantation of In and As into Si [4, 5]. That band was ascribed to the InAs nanocrystals. One can see in Fig. 4 that "hot" implantation of Si samples results in more effective luminescence in comparison with room temperature implantation.

4. Conclusions

We have demonstrated a possibility of producing InAs nanocrystals of the sizes from 2 to 600 nm in the Si and SiO_2 (40 nm)/Si structure by means of implantation of As^+ (170 keV, 3.2×10^{16} cm^{-2}) and then In^+ (250 keV, 2.8×10^{16} cm^{-2}) with subsequent thermal processing at 1050 °C for 3 min. It was shown that oxidation of the samples before thermal treatment results in impurity losses reduction, brings down broadening of depth concentration profiles, increases incorporation of impurity into the silicon lattice sites and enhances photoluminescence yield in the PL spectra.

For all samples a broad band in the region of 1.15–1.6 μm is registered. "Hot" implantation leads to more effective light emission in this spectral range in comparison with room temperature implantation. Oxidation of the sample before thermal treatment results in the increasing luminescence yield in the 1.15–1.6 μm spectral range.

References

[1] N.D. Zakharov, P. Werner, U. Gosele, *Appl. Phys. Lett.* **74**, 1701 (1999).

[2] G.E. Cirlin, N.K. Polyakov, V.N. Petrov, V.A. Egorov, V. Denisov, B.V. Volovik, V.M. Ustinov, Zh.I. Alferov, N.N. Ledentsov, R. Heitz, D. Bimberg, N.D. Zakharov, P. Werner, U. Gösele, *Mater. Phys. Mech.* **1**, 15 (2000).

[3] F.F. Komarov, L.A. Vlasukova, O.M. Milchanin, P.I. Gaiduk, V.N. Yuvchenko, S.S. Grechnyi, *Vacuum* **78**, 361 (2005).

[4] A.L. Tchebotareva, J.L. Brebner, S. Roorda, C.W. White, *Nucl. Instrum. Methods. Phys. Res. B* **175-177**, 187 (2001).

[5] F. Komarov, L. Vlasukova, W. Wesch, A. Kamarou, O. Milchanin, S. Grechnyi, A. Mudryi, A. Ivaniukovich, *Nucl. Instrum. Methods. Phys. Res. B* **266**, 3557 (2008).

[6] A.F. Komarov, F.F. Komarov, P. Zukowski, Cz. Karwat, A.A. Kamarou, *Vacuum* **63**, 495 (2001).

[7] F.F. Komarov, O.V. Milchanin, L.A. Vlasukova, W. Wesch, A.F. Komarov, A.V. Mudryi, *Bull. Russ. Acad. Sci., Phys.* **74**, 252 (2010).

[8] N.P. Barradas, C. Jeynes, R.P. Webb, *Appl. Phys. Lett.* **71**, 291 (1997).

[9] F. Komarov, L. Vlasukova, O. Milchanin, A. Komarov, W. Wesch, A.K. Togambaeva, *Lith. J. Phys.* **49**, 105 (2009).

[10] J.E. Rubio, M. Jaraiz, I. Martin-Bragado, P. Castrillo, R. Pinacho, J. Barbolla, *Mater. Sci. Eng. B* **124-125**, 392 (2005).